Curvature-insensitive methodology for thermal-wave depth-profilometry in multi-layered curvilinear solids

2010 J. Phys. D: Appl. Phys. 43 285403

(http://iopscience.iop.org/0022-3727/43/28/285403)

IOP PUBLISHING JOURNAL OF PHYSICS D: APPLIED PHYSICS

J. Phys. D: Appl. Phys. **43** (2010) 285403 (9pp) doi:10.1088/0022-3727/43/28/285403

Curvature-insensitive methodology for thermal-wave depth-profilometry in multi-layered curvilinear solids

Liwang Liu[1], Chinhua Wang[1], Xiao Yuan[1] and Andreas Mandelis[2]

[1] Key Lab of Modern Optical Technologies of Jiangsu Province, Institute of Modern Optical Technologies, Suzhou University, Suzhou, Jiangsu, 215006, People's Republic of China
[2] Center for Advanced Diffusion-Wave Technologies, Department of Mechanical and Industrial Engineering, University of Toronto, Toronto, Ontario, M5S 3G8, Canada

E-mail: chinhua.wang@suda.edu.cn

Received 4 March 2010, in final form 7 May 2010
Published 29 June 2010
Online at stacks.iop.org/JPhysD/43/285403

Abstract
A generalized similarity normalization (SN) methodology for characterizing depth profiles of continuously varying thermophysical properties in curvilinear (cylindrical and spherical) solids is presented. Specifically, the principle and the physical mechanism of the elimination of the surface curvature effect from the overall photothermal signal is introduced based on theoretical models of cylindrical, spherical and flat solids with multi-layer structures. The effects of the relative values of radii of curvature of the curvilinear solid, the thickness of the inhomogeneous surface layer and the measurement azimuthal angle on the validity of the technique are discussed in detail. Experimental reconstructions of thermophysical depth profiles of hardened cylindrical steel rods of various diameters are performed based on both curvilinear theory and the equivalent flat surface theory. The reconstructed results are compared and validated.

1. Introduction

Laser-induced photothermal radiometry (PTR) has become a powerful tool for the thermophysical characterization of broad classes of materials [1] since the late 1980s due to its non-destructive and highly sensitive nature. Most photothermal studies, however, have been limited to solids with flat surfaces due to the simplicity of geometry and the associated mathematical algorithms for which both one-dimensional [2, 3] and three-dimensional [4, 5] theoretical models have been developed and applied to various material studies. With increasing applications of PTR to materials characterization, recent studies have been extended to the evaluation of curvilinear samples. Wang *et al* developed models of homogeneous and 2-layer cylindrical and spherical samples, respectively [6–8], using the Green function method, in which the dependence of the photothermal field on both thermophysical and geometrical parameters of the sample (e.g. radius of curvature, azimuthal angle, etc) is obtained analytically. Salazar *et al* further developed the theory of multi-layer cylindrical and spherical samples for characterization of solids [9, 10] with discrete or continuously varying thermophysical properties. All those approaches establish theoretical bases for characterizing cylindrical and spherical solids if all the geometrical and measurement parameters are precisely known. This is a necessary prerequisite due to the complicated dependence of the photothermal signal on the geometrical shape, size and thermophysical properties [6–10]. Very recently, Liu *et al* [11] reported that geometrical factors, mainly the radius of curvature of cylindrical solids, can be eliminated or suppressed based on a similarity normalization (SN) method, which opens a new possibility of characterizing an arbitrarily curvilinear sample using well-developed analytical tools for flat solids. The SN was demonstrated experimentally using a set of hardened steel cylindrical rod samples with continuously varying thermophysical depth profiles along the radial direction. The mechanism was explained using homogeneous and bi-layer theoretical models to first-order approximation, in which the inhomogeneous layer was considered as an effective homogeneous layer. In this paper we present a detailed investigation (including both spherical and cylindrical solids)

of the methodology, optimization and comparison of results obtained by means of SN in curvilinear samples based on a multi-layer model that is more realistic than the bi-layer model for extracting thermophysical depth profiles of hardened steels. Especially, it was found that the effect of the measurement azimuthal angle on the PTR signal of curvilinear solids can also be eliminated or suppressed in addition to the radius of curvature. The sensitivity, optimization and the variation tolerance of the azimuthal angle on the SN method were studied in detail. The validity range of the SN technique in terms of the relative value of radius of curvature of the curvilinear sample, the thickness of the inhomogeneous surface layer and the measurement angle are discussed based on the more realistic multi-layered model. Experimental reconstructions of thermophysical depth profiles of hardened cylindrical steel rods with various diameters are presented based on both similarity-normalized curvilinear theory and the equivalent flat surface theory. The reconstructed results are compared and validated.

2. Theory

A case-hardened steel (with a flat, cylindrical, spherical or other curvilinear surface) may be a typical inhomogeneous structure with an outer hardened layer in which the radial thermophysical property (e.g. thermal conductivity and/or hardness) varies continuously down to a homogeneous unhardened inner layer. To precisely characterize these types of solids multi-layer theoretical models must be developed and employed for each type of curvature. The inhomogeneous layer is divided into N layers thin enough that each layer can be considered thermophysically homogeneous. When the number of layers is appropriately chosen (large enough), the multi-layer model can be a good approximation of a continuous model. Considering the thickness of the inhomogeneous hardened layer is generally of few millimetres maximal, $N \sim 30$ layers are usually sufficient to describe a continuous layer with good accuracy [12]. Special cases have been presented in previous papers [9, 10, 12]. More general thermal-wave inverse problem reconstruction techniques have been introduced over several years by our group [13]. Figure 1 shows the geometries and the coordinates of multi-layer cylindrical (figure 1(a)), spherical (figure 1(b)) and flat (figure 1(c)) structures, respectively. All three types of solids are assumed to consist of N layers. The thermophysical properties of the ith layer are labelled (k_i, α_i), where k_i and α_i are thermal conductivity and thermal diffusivity, respectively. In the cylindrical and spherical case the outer and inner radius of layer i is denoted by a_i and a_{i+1}, respectively, with the thickness of layer i being $L_i = a_i - a_{i+1} (i = 1 \ldots N-1)$. The curvilinear solids are illuminated with a uniform light beam impinging on part of their surface subtending a sector of angle 2Ω (shown in figures 1(a) and (b)). The flat solid is illuminated with a Gaussian laser beam of spot size w_0. When w_0 is large enough, the beam is essentially uniform to ensure the same uniform illumination in comparison with the cylindrical and spherical cases. The incident beam is intensity modulated at frequency f.

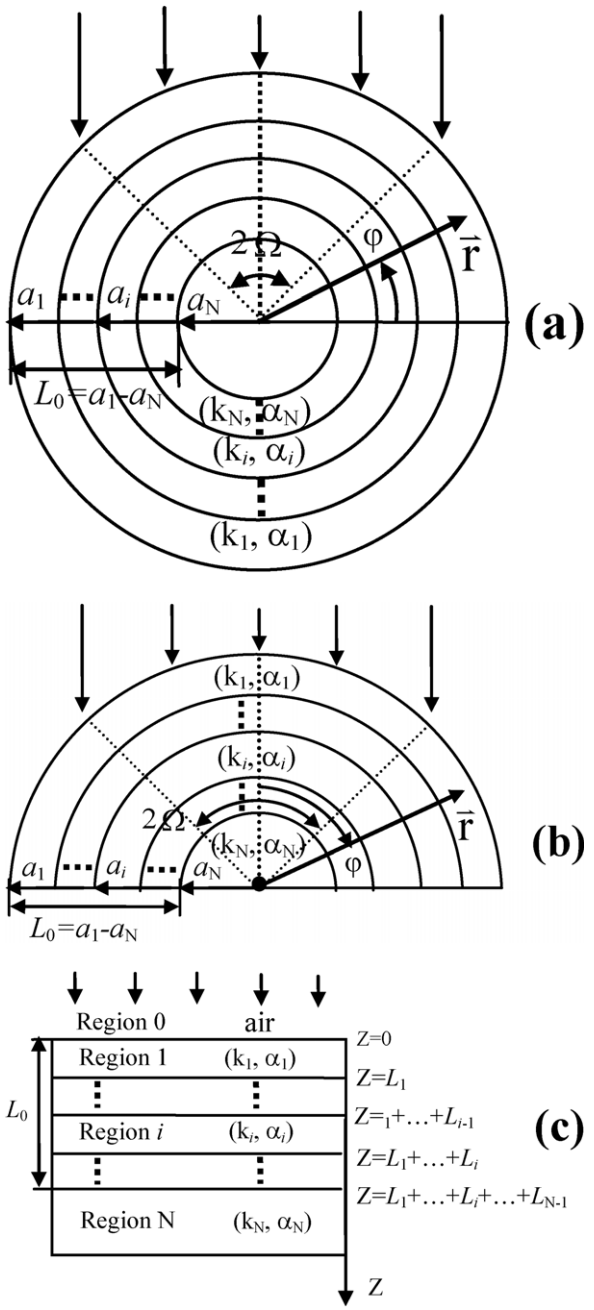

Figure 1. Geometry and coordinates of multi-layer cylinder (a), sphere (b) and flat (c) structures. All the three samples are assumed to consist of N layers.

For the cylindrical solid, the thermal-wave field on the surface ($r = a_1$) at azimuthal angle φ is given by [9]

$$T(a_1, \varphi) = \frac{I_0}{2} \sum_{m=-\infty}^{\infty} g_m(\Omega) \times \left(\frac{A'_m}{C'_m} \right) \mathrm{e}^{\mathrm{i}m\varphi}, \qquad (1)$$

where

$$g_m(\Omega) = (-i)^m \frac{m \sin(m\Omega)\cos(\Omega) - \sin(\Omega)\cos(m\Omega)}{\pi(m^2 - 1)}.$$

The coefficients A'_m, C'_m are obtained through a recursion relation:

$$\begin{pmatrix} A'_m & B'_m \\ C'_m & D'_m \end{pmatrix} = \prod_{i=1}^{N} \begin{pmatrix} A_{mi} & C_{mi} \\ B_{mi} & D_{mi} \end{pmatrix}, \quad m = -\infty, \ldots, 0, \ldots, +\infty, \tag{2}$$

where

$$\begin{aligned} A_{mi} &= [H'_{mi}(q_i a_{i+1}) J_{mi}(q_i a_i) - J'_{mi}(q_i a_{i+1}) H_{mi}(q_i a_i)]/E_{mi}, \\ B_{mi} &= [J_{mi}(q_i a_{i+1}) H_{mi}(q_i a_i) - H_{mi}(q_i a_{i+1}) J_{mi}(q_i a_i)] \\ &\quad /E_{mi} k_i q_i, \\ C_{mi} &= k_i q_i [H'_{mi}(q_i a_{i+1}) J'_{mi}(q_i a_i) - J'_{mi}(q_i a_{i+1}) H'_{mi}(q_i a_i)] \\ &\quad /E_{mi}, \\ D_{mi} &= [J_{mi}(q_i a_{i+1}) H'_{mi}(q_i a_i) - H_{mi}(q_i a_{i+1}) J'_{mi}(q_i a_i)]/E_{mi}, \\ E_{mi} &= H'_{mi}(q_i a_{i+1}) J_{mi}(q_i a_{i+1}) - H_{mi}(q_i a_{i+1}) J'_{mi}(q_i a_{i+1}). \end{aligned}$$

Here $q_i = \sqrt{j\omega/\alpha_i}$ ($\omega = 2\pi f$ is the angular frequency) is the complex thermal wavenumber of layer i; J_m,H_m and J'_m,H'_m are the Bessel and Hankel functions of the first kind of order m, and their derivatives, respectively.

For spherical samples, the thermal-wave field at the surface ($r = a_1$) is given by [10]:

$$T(a_1, \varphi) = \frac{I_0}{2} \sum_{n=0}^{\infty} g_n(\Omega) \times \left(\frac{A'_n}{C'_n} \right) P_n(\cos\varphi), \tag{3}$$

where P_n is the Legendre polynomial,

$$g_n(\Omega) = \frac{2n+1}{2} \int_0^{\Omega} P_n(\cos\lambda) \cos\lambda \, \sin\lambda \, \mathrm{d}\lambda,$$

I_0 is light intensity, and the coefficients A'_n, C'_n are given in [10] as follows:

$$\begin{pmatrix} A'_n & B'_n \\ C'_n & D'_n \end{pmatrix} = \prod_{i=1}^{N} \begin{pmatrix} A_{ni} & C_{ni} \\ B_{ni} & D_{ni} \end{pmatrix}, \qquad n = 0, \ldots, +\infty, \tag{4}$$

where

$$\begin{aligned} A_{ni} &= [h'_{ni}(q_i a_{i+1}) j_{ni}(q_i a_i) - j'_{ni}(q_i a_{i+1}) h_{ni}(q_i a_i)]/E_{ni}, \\ B_{ni} &= [j_{ni}(q_i a_{i+1}) h_{ni}(q_i a_i) - h_{ni}(q_i a_{i+1}) j_{ni}(q_i a_i)]/E_{ni} k_i q_i, \\ C_{ni} &= k_i q_i [h'_{ni}(q_i a_{i+1}) J'_{ni}(q_i a_i) - J'_{ni}(q_i a_{i+1}) H'_{ni}(q_i a_i)]/E_{ni}, \\ D_{ni} &= [j_{ni}(q_i a_{i+1}) h'_{ni}(q_i a_i) - h_{ni}(q_i a_{i+1}) j'_{ni}(q_i a_i)]/E_{ni}, \\ E_{ni} &= h'_{ni}(q_i a_{i+1}) j_{ni}(q_i a_{i+1}) - h_{ni}(q_i a_{i+1}) j'_{ni}(q_i a_{i+1}). \end{aligned}$$

Here $q_i = \sqrt{j\omega/\alpha_i}$ is the complex thermal wavenumber of layer i; j_m, h_m and j'_m, h'_m are spherical Bessel and Hankel functions of the mth order, and their derivatives, respectively.

For a flat rectilinear solid the thermal-wave field at the surface is given by [12]

$$T_1(r, z = 0, \omega) = \int_0^{\infty} \frac{Q_S(0)}{k_0 \delta_0 (1 + b_{1,0})} \cdot \frac{1 + g_1 \mathrm{e}^{-2\delta_1 L_1}}{1 + \gamma_{1,0} g_1 \mathrm{e}^{-2\delta_1 L_1}} \mathrm{e}^{-\frac{\lambda^2 w_0^2}{4}} J_0(\lambda r) \lambda \, \mathrm{d}\lambda, \tag{5}$$

where

$$Q_S(0) = \frac{A_S(1 - R_1)P}{\pi \omega_0^2} \mathrm{e}^{-r^2/w_0^2};$$

where R_1, A_S are the surface reflection and absorption coefficient, respectively. The coefficients g_1, $\gamma_{1,0}$ in equation (5) are calculated using a recursion relation as follows:

$$\begin{cases} g_i = \dfrac{1 - b_{i+1,i} p_{i+1}}{1 + b_{i+1,i} p_{i+1}}, & p_{i+1} = \dfrac{1 - g_{i+1} \mathrm{e}^{-2\delta_{i+1} L_{i+1}}}{1 + g_{i+1} \mathrm{e}^{-2\delta_{i+1} L_{i+1}}}, \\ b_{i+1,i} = \dfrac{k_{i+1} \delta_{i+1}}{k_i \delta_i}, & \delta_i^2 = \lambda^2 + \sigma_i^2, \\ \gamma_{1,0} = \dfrac{1 - b_{1,0}}{1 + b_{1,0}}, & g_N = \dfrac{1 - b_{M,N}}{1 + b_{M,N}}, \\ \sigma_i = (1 + j)\sqrt{\omega/2\alpha_i}. \end{cases}$$

To quantitatively characterize and/or reconstruct steel case hardness depth profiles by means of their relation to inhomogeneous thermophysical parameters of solids with a flat, cylindrical or spherical surface, a proper mathematical description of the thermal conductivity/diffusivity depth profile is needed. The assumed depth profile ansatz meets the following requirements: (1) the thermophysical parameters are a monotonic function of depth, z, with the possibility to increase or decrease; (2) the thermophysical profile saturates at a pre-determined depth to conform with the unhardened bulk of the sample and (3) the number of parameters involved in the ansatz is as small as possible to minimize the complexity of the computational best fit and fitting time. Equation (6) satisfies the assumed requirements [12, 13]:

$$k(z) = k_1 \left(\frac{1 + \Delta \mathrm{e}^{-Qz}}{1 + \Delta} \right)^2, \qquad \text{with } \Delta = \frac{1 - \sqrt{k_N/k_1}}{\sqrt{k_N/k_1} - \mathrm{e}^{-QL_0}} \tag{6}$$

where k_1 and k_N represent the values of the thermal conductivity at the two boundary surfaces $z = 0$ (sample surface) and $z = L_0$ (depth inside the sample at which the thermophysical parameters saturate to those of the bulk body), respectively. L_0 is the total thickness of the inhomogeneous surface layer. Equation (6) is capable of describing all possible monotonic curves with depth, which is adequate for expressing arbitrary monotonic profiles, if parameters are properly chosen. The depth profile of the thermal conductivity is determined by the combination of k_1, k_N, Q and L_0.

From the aforementioned theoretical models, it is analytically seen that the thermal-wave fields of cylindrical and spherical solids are inherently more complicated than that of the flat solid because of the dependence of the TW signal on the azimuthal angle and the diameter. In what follows, we will quantitatively discuss the effects of the geometrical factors on the thermal-wave signal and will present a method for the deconvolution of the geometrical parameters of curvilinear solids. The method introduces a geometry insensitive technique for characterizing depth profiles of solids with arbitrary curvatures and multi-layers.

3. Numerical calculations

3.1. Dependence of thermal-wave field on geometrical parameters of curvilinear solids

We first show the sensitive dependence of thermal-wave fields on geometrical parameters of cylindrical, spherical and flat

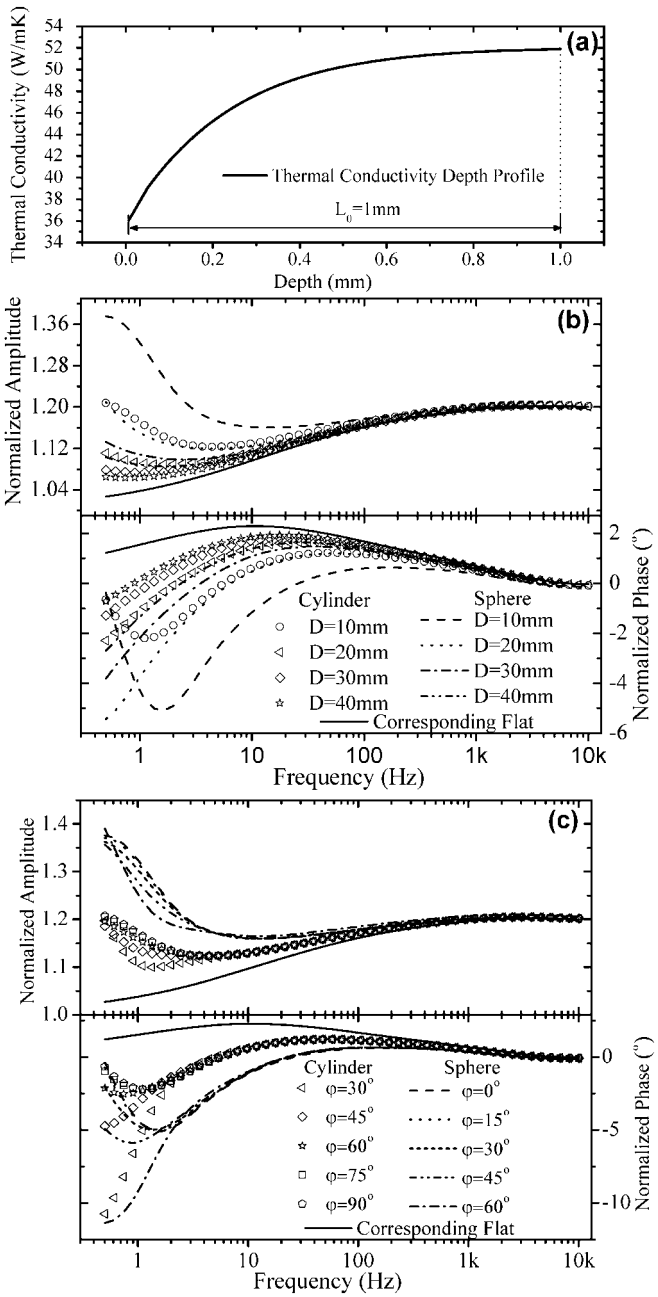

Figure 2. Thermal-wave field frequency response dependence on cylindrical, spherical and rectilinear (flat) solids. (*a*) Depth profile of thermal conductivity of the common inhomogeneous surface layer, calculated using equation (6) with $L_0 = 1$ mm, $Q = 4500\,\mathrm{mm}^{-1}$. (*b*) Amplitude and phase of thermal-wave field of the flat, cylindrical and spherical solids with various radii of curvature. (*c*) Amplitude and phase of thermal-wave fields at different azimuthal angles φ, figures 1(*a*) and (*b*).

solids. The depth profiles of the thermal conductivity along the radial direction of cylindrical and spherical solids are assumed to be identical to that of a rectilinear solid, represented by equation (6). Figure 2(*a*) shows the assumed thermal conductivity depth profile of the same inhomogeneous layer for all three types of cylindrical, spherical and flat solids, as if they all underwent the same carburizing process, although the sizes of the samples are different. In figure 2(*a*), $k_1 = 36.05\,\mathrm{W\,mK^{-1}}$, $\alpha_1 = 9.426 \times 10^{-6}\,\mathrm{m^2\,s^{-1}}$ at $z = 0$ (sample surface) and $k_N = 51.9\,\mathrm{W\,mK^{-1}}$, $\alpha_N = 13.57 \times 10^{-6}\,\mathrm{m^2\,s^{-1}}$) at $z = L_0$ (steel material AISI1018 is assumed [14]). The total thickness of the inhomogeneous layer (case-hardened layer) L_0 is assumed to be 1 mm. The exponent Q in equation (6) represents the thermal conductivity gradient and is assumed to be $4500\,\mathrm{mm^{-1}}$. Figure 2(*b*) shows the radius-of-curvature effect for various cylindrical and spherical samples on the thermal-wave signal frequency dependence and the comparison with that from the flat solid with the same depth profile. Normalization of the amplitudes and phases in figure 2(*b*) is done by amplitude division and phase subtraction of equations (1), (3) and (5) for inhomogeneous cylindrical, spherical and flat surfaces, respectively, by those of a semi-infinite flat unhardened (homogeneous) AISI1018 steel sample. The amplitude and phase of the semi-infinite flat solid sample are calculated based on the well-known 1D theoretical model [2]:

$$T(0,\omega) = F_0[\sqrt{\alpha}/(k\sqrt{\omega})]\exp(-\mathrm{i}\pi/4), \qquad (7)$$

where k and α are thermal conductivity and thermal diffusivity, respectively, of the homogeneous solid. This normalization has the additional benefit of eliminating the instrumental transfer function from experimental data processing. Theoretically, cylinders and spheres with diameters $D = 10$, 20, 30 and 40 mm and the corresponding inhomogeneous flat solids were investigated. The azimuthal angle φ as fixed at 90° and 0° for cylinders and spheres, respectively, figure 1. For a fixed inhomogeneous depth profile, thermal-wave signals of different radii of curvature show different frequency responses. The smaller the radius of curvature, the larger the deviation from the flat solid, as expected. The sensitivity of the thermal-wave signal on the measurement azimuthal angle (φ) is shown in figure 2(*c*). It should be noted that the definition of azimuthal angle (φ) for cylinders and spheres is different and shown in figures 1(*a*) and (*b*). The (common) diameter of the cylinder and sphere with the same thermal conductivity depth profile, figure 2(*a*), was assumed to be 10 mm. From figure 2(*c*), it is obvious that the thermal-wave signal is very sensitive to φ, especially at low frequencies. Furthermore, the thermal-wave responses from cylinders and spheres at a given azimuthal angle are different from that of the corresponding flat solid. In all these simulations in figures 2(*b*) and (*c*), the laser beam size was assumed to be large enough, i.e. subtend an angle $2\Omega = 180°$, so as to cover the entire upper part of the cylinder and sphere, thereby also meeting the 1D condition as in the case of the flat solid.

3.2. Elimination of geometrical effects in the TW response of cylinders and spheres

The SN resulting in the approximate suppression of the radius of curvature of cylindrical and spherical solids from their thermal-wave frequency response has been explained [11] using uniform and bi-layer theoretical models, which is adequate for a thin two-layer structure. For more general cases such as a multi-layer or continuously inhomogeneous media (e.g., a case-hardened steel layer), the multi-layer theoretical

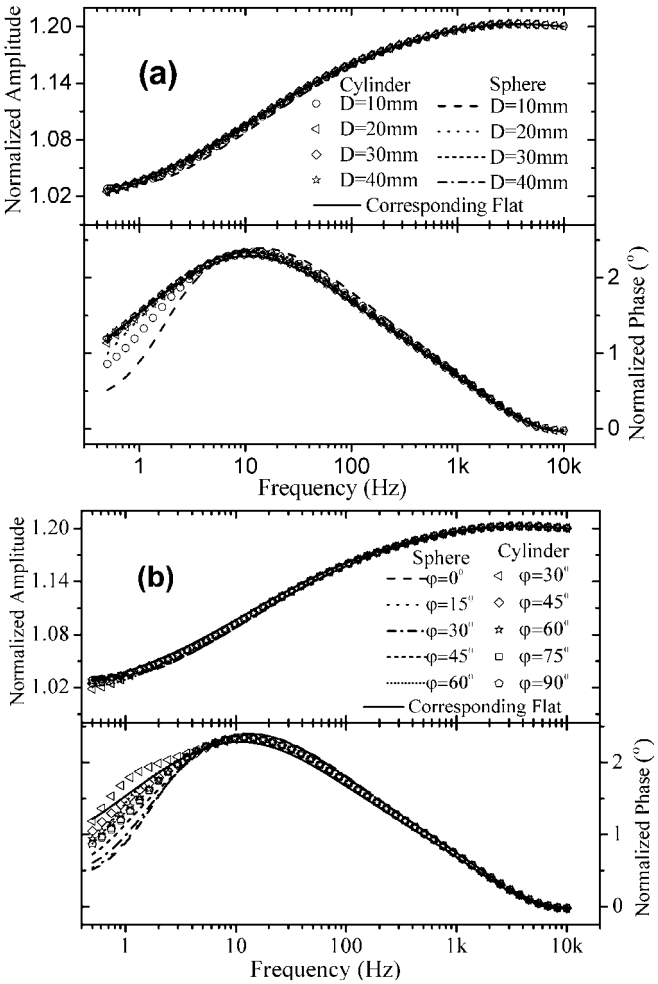

Figure 3. (*a*) Normalized amplitude and phase of thermal-wave fields of cylindrical and spherical samples with different radii of curvature and that of the corresponding flat sample. (*b*) Normalized amplitude and phase of thermal-wave fields at different azimuthal angles φ, figures 1(*a*) and (*b*).

models introduced in this work must be used. From the mathematical expression shown in equation (1) (cylinders) or equation (3) (spheres), it is seen that the dependence of the thermal-wave field on geometrical parameters (radius of curvature, azimuthal angle and beam-subtending angle) of a homogeneous cylinder (sphere) and their multi-layer counterparts is similar, with the only difference being the A'_n and C'_n related terms which carry information on depth inhomogeneity of the thermal-wave fields of composite solids and act as coefficients of otherwise identical angular functions. With the same outer radius a_1, the aforementioned normalization process of the thermal-wave field in a curvilinear multi-layer solid with respect to that of the corresponding homogeneous cylindrical (spherical) solid can essentially eliminate the dependence of the thermal-wave field on the radius of curvature and the azimuthal angle φ, curvilinear parameters which otherwise affect the behaviour of the thermal-wave field as shown in figures 2(*b*) and (*c*). Figure 3 shows the details of curvature elimination based on the homogeneous and multi-layer cylindrical and spherical models. In the calculation, the thermal conductivity and diffusivity depth profiles of the inhomogeneous layer in figure 2(*a*) were employed. The other solid parameters (radius of curvature and azimuthal angle) were exactly the same as those in figure 2(*b*). The normalization was performed using multi-layered solid (cylinder or sphere) normalization with respect to the corresponding homogeneous counterparts with the same outer diameter. The thermophysical parameters of these homogeneous solids as well as those of the central region of the inhomogeneous solids were assumed to be unhardened AISI1018 steel, i.e. $k_N = 51.9\,\mathrm{W\,mK^{-1}}$ and $\alpha_N = 13.57 \times 10^{-6}\,\mathrm{m^2\,s^{-1}}$. It is seen in figure 3(*a*) that the normalized amplitudes of solids with different diameters, including the flat solid, essentially coincide in the entire frequency range. This is in sharp contrast to figure 2(*b*). This phenomenon can also be seen in figure 3(*b*) in which the diameters of the cylinder and sphere are fixed at 10 mm while the angle φ is varied. These results indicate that effects of radius of curvature and azimuthal angle of cylindrical and spherical solids can be eliminated from photothermal amplitudes using the aforementioned normalization process. The significance of curvature and azimuthal angle elimination is that the curvilinear solid can be characterized using the current existing and considerably simpler techniques for flat solids. Nevertheless, a residual memory of the curvature and angle of measurement can be seen in the phase channel especially for small radii of curvature in the low frequency range < 5 Hz. Therefore, next we will discuss the curvature suppression validity range from the thermal-wave frequency response using the aforementioned normalization process in detail.

3.3. Validity range and geometry suppression tolerance

The frequency range validity of radius-of-curvature suppression, or the degree of equivalence of curvilinear to flat solids, depends mainly on the relative values of the thickness of the inhomogeneous layer and the radius of curvature of the curvilinear solid. Figure 4 shows the suppression effect of cylindrical curvature with a fixed outer diameter but different thicknesses (depth profiles) of the inhomogeneous layer. The corresponding thermal-wave fields of flat solids with the same depth profile are also shown. In the calculation, the outer diameter of the cylinders is fixed at 10 mm. Four different thermal conductivity depth profiles are assumed with (k_1, α_1) at the surface and (k_N, α_N) inside the core of the solids. They are the same as those of figure 2 with $Q = 10\,000\,\mathrm{mm^{-1}}$, $6000\,\mathrm{mm^{-1}}$, $4000\,\mathrm{mm^{-1}}$ and $3000\,\mathrm{mm^{-1}}$ and $L_0 = 0.5$ mm, 1.0 mm, 1.5 mm, 2.0 mm, respectively. It is seen that different ratios of inhomogeneous layer thicknesses over radii of curvature result in different degrees of curvature suppression. A ratio factor $\chi = (a_1 - a_N)/a_1$ is defined as the measure of the relative thickness of the inhomogeneous layer $L_0 (= a_1 - a_N)$ and the radius of curvature (a_1) of cylinder or sphere.

To quantitatively show elimination, the deviation factor is defined [11] as

$$\Delta_x = \sqrt{\sum_{j=1}^{N} (X_{j,\mathrm{cylinder}} - X_{j,\mathrm{flat}})^2 / N} / (X_{\max} - X_{\min})_{\mathrm{flat}}$$

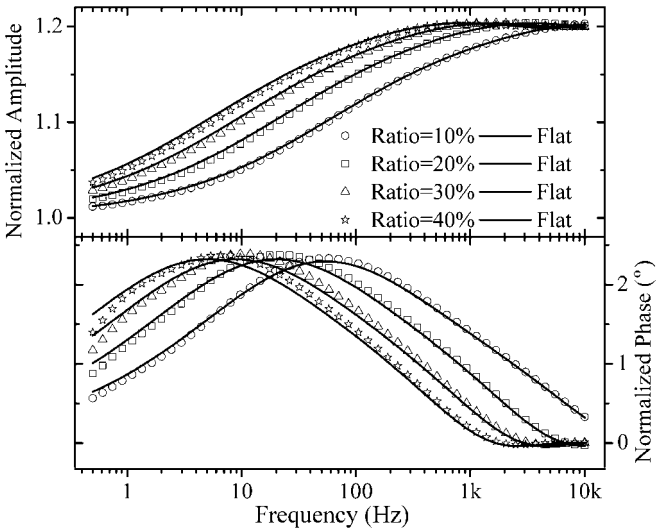

Figure 4. Equivalence of multi-layered cylinders with a fixed diameter ($2a_1 = 10$ mm) and various thicknesses of the inhomogeneous layer to the corresponding flat solids. Ratio $\chi = (a_1 - a_N)/a_1$ with a_N being the inner layer radius. Symbols: cylindrical solid; solid lines: flat solid.

and represents the average deviation from the corresponding SN flat surface in either amplitude or phase channel ($X = A$, φ, respectively). $N = 51$ is the number of frequency scanned points. The effect of Δ_x is shown in figure 4. In that figure Δ_A is 0.68%, 2.1%, 3.3% and 5.4%, whereas Δ_φ is 1.8%, 2.1%, 4.7% and 6.8% for $\chi = 10\%$, 20%, 30% and 40% , respectively. This indicates that the smaller the ratio is, the better the suppression of the curvature effect, which can also be seen clearly at low frequencies in figure 4. Significant discrepancy between the curvilinear and the flat surface appears as the ratio increases to ∼40%, especially in the phase channel where the important featured peak position of the cylindrical solid may shift away from that of the flat surface sample. From figure 4, it is estimated that the validity range of the ratio (L_0/a_1) is around 30% if 5% of experimental uncertainty is assumed.

It is seen that curvature suppression is very efficient in the high frequency range while the discrepancies due to curvature appear in both amplitude and phase channels, especially in the low frequency range (below the peak frequency) for samples with small radius of curvature. The lower limit of the SN validity frequency range is related to the peak frequency in the phase channel which depends on the thickness of the inhomogeneous top layer of the solid as described in [11]: the thicker the top layer the lower the frequency of the peak, which can be explained by the larger thermal diffusion length (lower frequency) required to detect the thicker coating layer through interlayer thermal-wave interference. However, it is found that choosing an appropriate azimuthal measurement angle can improve the curvature suppression effect or broaden the SN validity frequency range as shown in figure 5. Figure 5 shows the effect of curvature for various diameters (4 mm, 6 mm, 12 mm and 18 mm) of cylindrical solids as a function of variation in azimuthal angle φ. The thermal conductivity depth profile and the thermophysical parameters are the

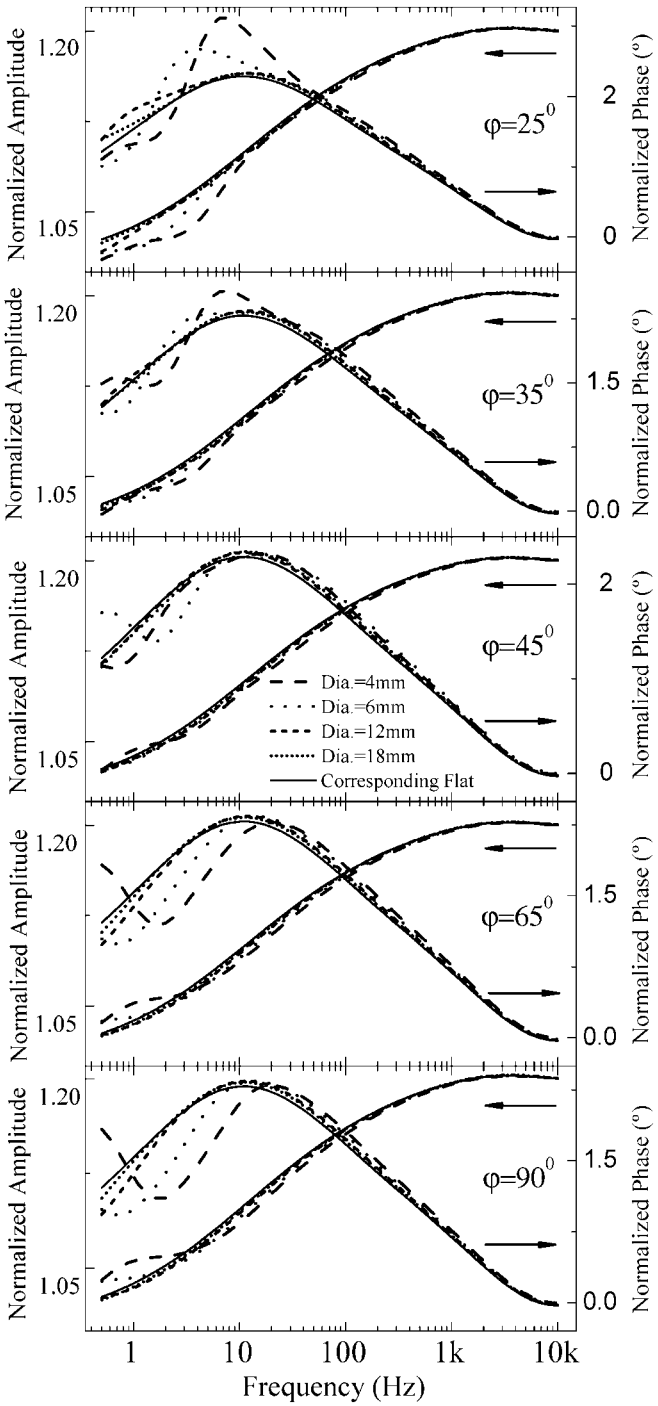

Figure 5. Curvature effect suppression in cylinders of various diameters as a function of azimuthal angles φ, figure 1(a).

same as those used in figure 2. From figure 5, it is seen that curvature effects can be suppressed completely at high frequencies at all azimuthal angles. At low frequencies below the peak frequency, however, different angles exhibit different suppression efficiencies: the optimum azimuthal angle is 45°. Besides, the valid frequency range is broadened when choosing the azimuthal angle at 45°. For example, in the case of the 4 mm solid (dashed line in figure 5), the lower limit of the SN validity frequency range is about 30 Hz, 20 Hz, 4 Hz, 10 Hz and 20 Hz when the azimuthal angle is 25° , 35° , 45°, 65° and 90°,

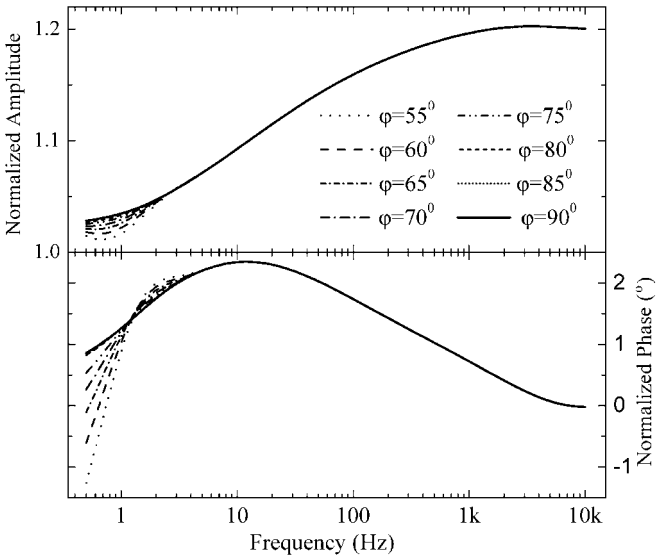

Figure 6. The effect of azimuthal angle deviations between the inhomogeneous and the homogeneous cylindrical solid. φ of the homogeneous cylindrical solid is fixed at 90° while that of the homogeneous solid is varied from 55° to 90°.

respectively. This indicates that it is better to set the azimuthal angle at 45° when using the SN method to characterize the thermophysical property of cylindrical samples.

The essence of suppressing geometrical factors lies in the normalization process of solids of the same size and shape with either inhomogeneous or homogeneous thermophysical property depth profiles. In terms of experimental implementation, proper positioning of the curvilinear sample with either inhomogeneous or homogeneous depth profile in the experimental set-up is crucial for accuracy of the technique. To indicate sensitivity to sample positioning, figure 6 shows the effect of various deviations of the azimuthal angle between an inhomogeneous and a homogeneous cylindrical solid. In the calculation, the azimuthal angle of the homogeneous cylinder is fixed at 90°, while the azimuthal angle of the inhomogeneous solid is varied from 55° to 90°, simulating the positioning error in the experiments. In the simulation, the diameter of the solid is assumed to be 10 mm and the thermal conductivity depth profile of figure 2(*a*) is employed. Both normalized amplitude and phase with various deviations in azimuthal angle between homogeneous and inhomogeneous solids show good or excellent consistency, especially in the high frequency range. Within the range ∼15°–20° deviation in azimuthal angle, the effect of sample misalignment can approximately be ignored at frequencies above 1 Hz. This is very significant for real-time industrial applications: the high tolerance in sample alignment makes the measurement more convenient and practical.

4. Experimental results

Two sets of cylindrical AISI 1020 steel samples were machined with diameters of 4, 10 and 16 mm. The length of the samples is ∼4 cm. The cylindrical samples stand on a sample holder freely and vertically. The measuring point on the cylindrical

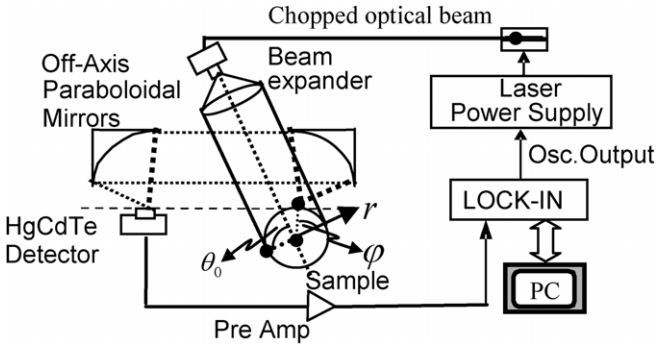

Figure 7. Experimental PTR set-up.

sample is far away from the contacting boundary between the standing end of the sample and the holder, so thermal contact can be negligible. One set of samples underwent a case hardening (carburizing) process together as one batch to ensure the same case depth profile, with a nominal case depth 0.04 inch, while the other set of samples was kept unhardened (reference). Thermophysical properties of AISI 1020 steel are as follows: $k_N = 50.63\,\mathrm{W\,mK^{-1}}$, $\alpha_N = 13.7663 \times 10^{-6}\,\mathrm{m^2\,s^{-1}}$. The experimental PTR set-up of figure 7 was employed and the north pole point of the cylindrical rods, i.e. with 90° azimuthal angle, was adopted. It should be noted that the PTR signal of flat solids was obtained by measuring the bottom (flat) surface of 16 mm diameter cylindrical samples, and the beam size was expanded to around 18 mm so as to meet the conditions of the 1D theoretical model. Experimental results have been reported in [11], and the results show good agreement with the theoretical simulations. Normalized amplitudes and phases obtained from curvilinear samples with various diameters overlap with the corresponding flat solid; however, both amplitude and phase of different diameters show discrepancies at the low frequency range, especially for small diameters. For comparison, we fitted the experimental data on the basis of two different theoretical models and the results are shown in figure 8 while the detailed best-fit parameters are shown in tables 1(*a*) and 1(*b*). It is seen that all best-fitted results, regardless of model (cylindrical or flat solid), show good agreement with data from the 10 mm and 16 mm diameter samples. Particularly for the 4 mm diameter cylinder, while the cylindrical theoretical model can fit the experimental data very well, including the valley in the phase channel at low frequencies, the rectilinear theoretical model exhibits obvious disagreement especially in the phase channel at low frequencies. This is because the ratio χ reaches about 50%, that is, far beyond the upper limit of the validity range (30%) discussed in section 3.3.

Figure 9 shows the comparison of the reconstructed thermal conductivity depth profiles based on the two different theoretical models. From the reconstructed hardness case depth profiles based on the cylindrical theoretical model (figure 9(*a*)) and the multi-layered rectilinear model, figure 9(*b*), it is seen that thermal conductivity profiles of rods with various diameters all approximately coincide with that of the flat solid no matter the diameters of the cylinders and which theoretical model is used for reconstruction. This

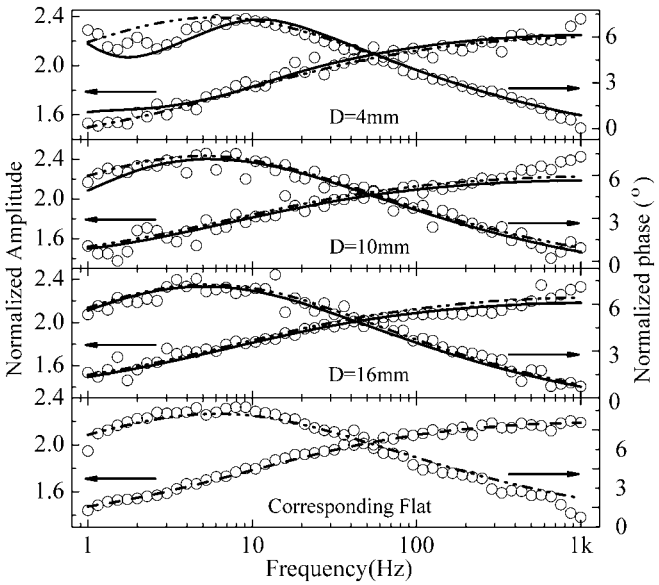

Figure 8. Comparisons of the best-fitted results of experimental data on the basis of the cylindrical theoretical model (solid line) and flat theoretical model (dashed line). Symbols denote experimental curves.

Table 1(*a*). Best-fit result of cylindrical rods based on cylindrical model.

Sample diameter (mm)	k_1 (W mK^{-1})	L_0 (mm)	Q (mm^{-1})	φ Degree
4	15.06	1.05	3100	80.7
10	16.49	1.15	3610	82.6
16	16.46	1.07	3580	85.0

Table 1(*b*). Best-fit result of cylindrical rods based on rectilinear (flat) model.

Sample diameter (mm)	k_1(W mK^{-1})	L_0(mm)	Q(mm^{-1})
4	15.55	0.95	4805
10	15.93	0.98	3475
16	15.79	1.02	3666
Flat	15.34	1.08	3975

is consistent with the theoretical demonstration and indicates that a curvilinear cylindrical depth profile can be characterized using the algorithm for a flat solid. This phenomenon was also observed in [15] in which different shapes of screw samples have the same depth profile after undergoing the same carburizing hardening process in the same batch.

5. Conclusions

In summary, we have performed a detailed and comprehensive investigation on the thermal-wave equivalence of thermophysical property depth profiles between curvilinear and rectilinear (flat) solids based on theoretical models of cylindrical, spherical and flat solids with multi-layer structures. The curvature effect can be suppressed or eliminated by an appropriate normalization procedure (SN) depending on the ratio of the thickness of the inhomogeneous layer to the radius of the cylinder: the smaller the ratio, the better the SN equivalence. Compared with that described in [11] which uses a two-layer cylindrical model, the validity range of the ratio (L_0/a_1) can reach 30%, in contrast to ∼15% in the two-layer theory, if 5% of experimental uncertainty is assumed. The effect of the measurement azimuthal angle was discussed in detail. It was also found that the effect of the measurement azimuthal angle on the PTR signal of curvilinear samples can be eliminated or suppressed in addition to that of the radius of curvature. The curvature in the low frequency range, <10 Hz, may not obey the SN equivalence, especially for small diameter solids, but the equivalence can be improved by choosing an appropriate azimuthal angle optimized at 45°. In addition, the effect of azimuthal angle deviation due to sample positioning error in experimental implementation was studied. It was shown that within the range ∼15–20° deviation in azimuthal angle, misalignment of the sample can approximately be ignored. This is of practical significance for convenient and accurate measurements. The SN equivalence was further validated experimentally using PTR detection from a series of case-hardened steel cylinders and their flat surface counterparts with the same case-hardened profiles. The thermophysical depth profiles of rods reconstructed using a cylindrical theoretical model approximately coincide with those of the corresponding flat solid. In conclusion, curvilinear solids can be characterized using existing inversion techniques for flat solids on the basis of the SN presented in this paper. This is significant in that it enables the application of photothermal depth profilometric techniques, and PTR in particular, to inhomogeneous solids of cylindrical and spherical geometry. The extension of the method to arbitrary curvilinear geometries is under further investigation.

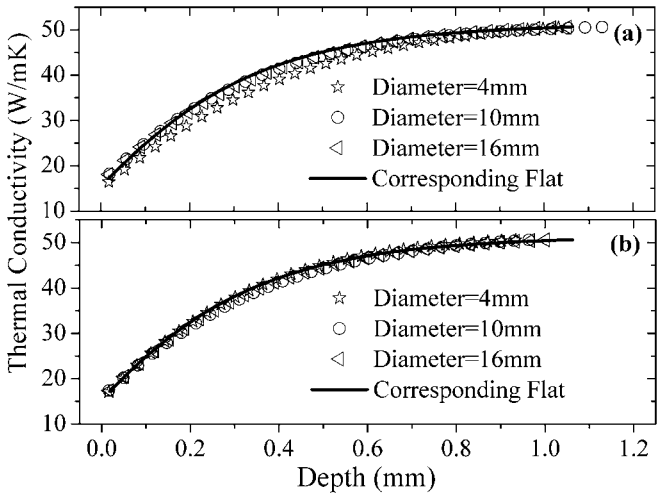

Figure 9. Comparison of the recovered thermal conductivity depth profile based on the cylindrical theoretical model (*a*) and the flat theoretical model (*b*).

Acknowledgments

This work has been sponsored by the National Natural Science Foundation of China (Grant No 60877063) and

Scientific Research Foundation for the Returned Overseas Chinese Scholars, State Education Ministry of China. XY acknowledges the support of NSAF (No 10676010, 10876011). One of them (AM) is grateful to the Canada Foundation for Innovation (CFI) and the Ontario Research Fund (ORF) for support with the experimental programme that made this research possible.

References

[1] Almond D P and Patel P M 1996 *Photothermal Science and Techniques* (London: Chapman and Hall)
[2] Mandelis A 2001 *Diffusion-Wave Fields: Mathematical Methods and Green Functions* (New York: Springer)
[3] Santos R and Miranda L C M 1982 *J. Appl. Phys.* **53** 5392
[4] Fabbri L and Fenici P 1995 *Rev. Sci. Instrum.* **66** 3593
[5] Qian L and Li P Z 1990 *Acta Optica Sinica* **3** 13
[6] Wang C, Mandelis A and Liu Y 2004 *J. Appl. Phys.* **96** 3756
[7] Wang C, Mandelis A and Liu Y 2005 *J. Appl. Phys.* **97** 014911
[8] Xie G, Chen Z, Wang C and Mandelis A 2009 *Rev. Sci. Instrum.* **80** 034903
[9] Salazar A and Celorrio R 2006 *J. Appl. Phys.* **100** 113535
[10] Madariaga N and Salazar A 2007 *J. Appl. Phys.* **101** 103534
[11] Liu W, Wang C, Yuan X and Mandelis A 2010 *J. Appl. Phys.* **107** 053503
[12] Hong Q, Wang C, Guo X and Mandelis A 2008 *J. Appl. Phys.* **104** 113518
[13] Mandelis A, Funak F and Munidasa M 1996 *J. Appl. Phys.* **80** 5570
[14] Steiner R 1990 *Metals Handbook* 10th edn (Materials Park, OH: ASM International) vol 1, p 196
[15] Wang C and Mandelis A 2007 *NDT & E Int.* **40** 158